Coincidence spectroscopy of molecular normal Auger decay by ultrashort x-ray pulses

Yan Ping Zhu,[1] Xi Zhao,[1] Xiao-Jing Liu,[2] Victor Kimberg,[3,*] and Song Bin Zhang[1,†]

[1]*School of Physics and Information Technology, Shaanxi Normal University, Xi'an 710119, China*

[2]*School Physical Science and Technology, ShanghaiTech University, Shanghai 201210, China*

[3]*Theoretical Chemistry and Biology, Royal Institute of Technology, Stockholm 10691, Sweden*

(Received 21 April 2022; accepted 5 August 2022; published 9 August 2022)

When a core-shell electron is ionized by coherent ultrashort x-ray pulses with varied duration, different nuclear wave packets of a cationic molecule are formed, which can be effectively studied by detecting the photoelectron-Auger electron-ion fragment as it is proposed in the present paper. We develop the theory for the photoelectron, i.e., Auger electron, ion fragment three-body coincidence spectroscopy, where dissociative Auger final states are considered. Simulations to display the HF molecule show that the coincidence spectra encode the detailed information of coherent nuclear wave-packet dynamics. Our work paves the way for using currently available coherent ultrashort x-ray pulses to investigate and manipulate molecular nuclear wave packets. Moreover, we discuss possibilities for high-resolution coincidence experimental techniques.

DOI: 10.1103/PhysRevA.106.023105

I. INTRODUCTION

Upon x-ray core-shell photoionization in tens of attoseconds, normal Auger decays happen within a few femtoseconds and produce dicationic molecular final states (Fig. 1). The Auger electron spectra imprint the information of both the electronic structures and core-shell electron correlations of the ionized molecule [1–7], which could be applied for element identification and structural analysis of large composite systems [8]. High-resolution Auger electron spectra also provide a versatile way to investigate the nuclear dynamics of both core-shell excited cation and valence states of dicationic molecules [9,10].

Various recently developed coincidence spectroscopic techniques provide powerful tools for investigation of different core-ionization induced dynamics with a number of degrees of freedom [11]. Namely, the photoelectron and Auger electron coincidence spectroscopy offers a possibility to disentangle the Auger electron spectra stemming from different intermediate ionic states [12–14], which otherwise overlap in the same energy region. These state-selective Auger electron spectra also allow for a better separation of the final states of the decay process, which cannot be achieved by other spectroscopic techniques [15]. Using various electron-electron coincidence setups at a synchrotron radiation source, Viefhaus *et al.* showed the interference effects between the photoelectron and Auger electron in atomic Xe [16], Ulrich *et al.* separated contributions from different vibrational levels in the C $1s^{-1}$ core-hole intermediate state to the Auger decay states of CO molecule [17], Prümper *et al.* studied whether the emission of the CO carbon KVV Auger electron is affected by photoelectron energy [18], and so on. In a complementary way, Auger channels can also be separated using the joint photoelectron–ion energy spectrum [19]. Besides that, resonant Auger electron–ion coincidence spectroscopy of N $1s \rightarrow \pi^*$ excitation from N_2 [20] and O $1s \rightarrow 4p\sigma$ excitation from O_2 [21] are also investigated. It is worth noting that Frasinski *et al.* studied covariance mapping: a correlation method applied to multiphoton multiple ionization [22]. Recently, Fushitani *et al.* studied multielectron–ion coincidence spectroscopy of Xe in extreme ultraviolet laser fields by using this method [23].

In this work, the concept of coincidence spectroscopy to probe core-hole coherent nuclear wave packets in the normal Auger process by coherent ultrashort x-ray pulses is proposed, together with the corresponding concise quantum dynamic theory. Different from the conventional monochromatic synchrotron radiation light source, x-ray free-electron laser (XFEL) facilities are known as sources of intense and ultrashort x-ray pulses [24–28], providing new opportunities for nonlinear [29–33] and time-resolved x-ray spectroscopy [34] and quantum manipulation in the x-ray region [2–4,35–37]. An increasing number of XFEL facilities are now focusing on delivering coherent (close to the Fourier transform limit) and short x-ray pulses using the so-called self-seeding technique [38], e.g., FERMI in Trieste, LCLS in Stanford, XFEL at Pohang Accelerator Laboratory, and SACLA in Japan. Moreover, application of the covariance analysis [39,40] allows us to make use of the traditional stochastic self-amplified spontaneous emission XFEL pulses [38] for the study of coherent processes with the help of statistical analysis and has been already successfully applied for XFEL experiments. As illustrated in Fig. 1, after kicking off one core-shell electron by a broadband ultrashort x-ray pulse, different coherent nuclear wave packets of the core-excited cation molecule can be created corresponding to photoelectrons of different energies; the rapid Auger decay dynamics followed will in turn depend on the nuclear wave-packet dynamics in both core-hole and final dication states.

*kimberg@kth.se

†song-bin.zhang@snnu.edu.cn

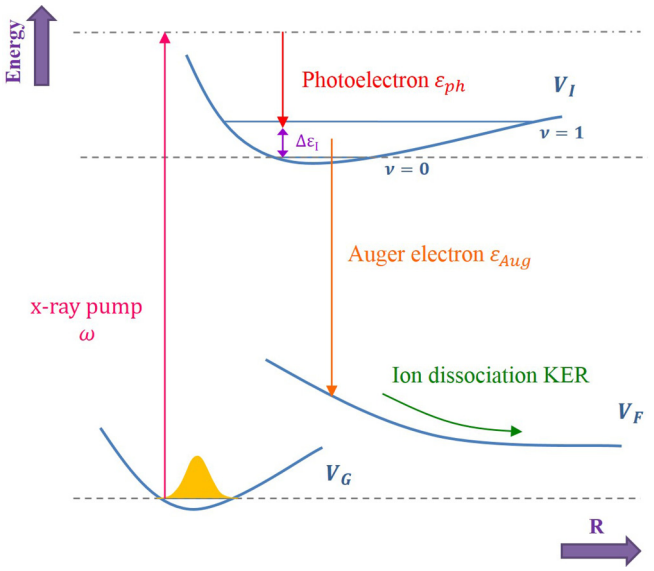

FIG. 1. Illustration of the normal Auger process following x-ray photoionization. The molecule in the ground state V_G is photoionized to the core-hole cation state V_I by an ultrashort x-ray pulse with central frequency ω, accompanied by the release of a photoelectron with energy $\varepsilon_{\rm ph}$; Auger decay happens and releases an Auger electron with energy $\varepsilon_{\rm Aug}$ when the system decays to the final dissociative dication state V_F. Ion fragments are also released carrying kinetic energies in the dissociative dication state. The coherent vibrational wave packet in the state V_I is created by the ultrashort pulse, changing the subsequent Auger decay dynamics and Auger electron spectra.

In order to reconstruct coherent nuclear wave-packet dynamics in the core-hole and final dissociative dication states, the three-body (photoelectron, Auger electron, and ion fragment) coincidence spectroscopy is implemented. Few-femtosecond x-ray pulses with bandwidths of around 1 eV are applied to excite a coherent superposition of a number of vibrational states creating a vibrational wave packet. High-resolution spectrometers to resolve and disentangle the contribution from different vibrational levels and correspondent interference structures are required, which could be challenging progress for implementation of the suggested experimental techniques. In addition, multicoincidence measurement becomes increasingly challenging with the complexity of the sample molecule, which could limit the feasibility of these techniques to small molecules.

The quantum theory of the process discussed is introduced in Sec. II. Section III presents the results and a discussion of the HF molecule. A summary is given in Sec. IV. Unless stated otherwise, atomic units ($e = m_e = \hbar = 1$) are used throughout the paper.

II. THEORETICAL METHODS

The time-dependent wave-packet propagation method was used to study the Auger electron spectrum (AES) and the kinetic energy release (KER) spectrum [31,36,41,42]. In the process studied here, the molecule is promoted by a coherent x-ray pulse with central frequency ω from the ground state G to the core-ionized state I, which is followed by the Auger decay to the final dication state F with emission of an electron with energy $\varepsilon_{\rm Aug}$. We label the electronic wave function and nuclear wave packet as $\Phi_G(\mathbf{r}, R)$ and $\Psi_G(R, t)$, $\Phi_I^{\varepsilon_{\rm ph}}(\mathbf{r}, R)$ and $\Psi_I^{\varepsilon_{\rm ph}}(R, t)$, and $\Phi_F^{\varepsilon_{\rm Aug}}(\mathbf{r}, R)$ and $\Psi_F^{\varepsilon_{\rm ph},\varepsilon_{\rm Aug}}(R, t)$ for the states G, I, and F, respectively, where R is the internuclear distance.

Previous work has described the theory for the case of resonant Auger scattering (RAS), where the intermediate state of the process is the core-excited neutral molecular state and one free electron is involved in the dynamics [31,36,41,42]. In the present work, we further develop this method, which then can be applied also for the description of the normal Auger process with two-free-electron dynamics. Since the photoelectron and Auger electron are distinguishable from their quite different kinetic energies, their correlation should be negligible and they could be treated as different particles. Moreover, here we neglect the postcollision interaction effect [43,44], as it is expected to be rather small in the present molecule far from the ionization threshold. In this case, the total wave packet of the normal Auger process can be written as

$$\Psi(\mathbf{r}, R, t) = \Psi_G(R, t)\Phi_G(\mathbf{r}, R) + \int \Psi_I^{\varepsilon_{\rm ph}}(R, t)e^{-i\omega t} \times \Phi_I^{\varepsilon_{\rm ph}}(\mathbf{r}, R)d\varepsilon_{\rm ph} + \iint \Psi_F^{\varepsilon_{\rm ph},\varepsilon_{\rm Aug}}(R, t)e^{-i\omega t} \times \Phi_F^{\varepsilon_{\rm Aug}}(\mathbf{r}, R)\Phi_I^{\varepsilon_{\rm ph}}(\mathbf{r}, R)d\varepsilon_{\rm Aug}d\varepsilon_{\rm ph}, \quad (1)$$

where the second and third terms indicate the wave functions for the ionic core state–photon electron and dication state–Auger electron–photon electron, respectively. A rapidly evolving phase factor $e^{-i\omega t}$ is explicitly separated [31,36,41]. Using the above total wave packet (1), following the techniques used in the resonant Auger process [31,41], the time-dependent Schrödinger equation can be transformed into a set of working equations depending on $\varepsilon_{\rm Aug}$ and $\varepsilon_{\rm ph}$, by employing the rotating-wave approximation [45–47] and the local approximation [48–51] twice (first over $\varepsilon_{\rm ph}$ and then over $\varepsilon_{\rm Aug}$), as

$$i\frac{\partial}{\partial t}\Psi(\varepsilon_{\rm ph}, \varepsilon_{\rm Aug}, R, t) = \hat{H}(\varepsilon_{\rm ph}, \varepsilon_{\rm Aug}, R, t)\Psi(\varepsilon_{\rm ph}, \varepsilon_{\rm Aug}, R, t), \quad (2)$$

where

$$\Psi(\varepsilon_{\rm ph}, \varepsilon_{\rm Aug}, R, t) = \left[\Psi_G(R, t), \Psi_I^{\varepsilon_{\rm ph}}(R, t), \Psi_F^{\varepsilon_{\rm ph},\varepsilon_{\rm Aug}}(R, t)\right]^T \quad (3)$$

and the total Hamiltonian is expressed as

$$\hat{H}(\varepsilon_{\rm ph}, \varepsilon_{\rm Aug}, R, t) = \hat{T}(R) + \begin{pmatrix} V_G(R) - \frac{i\Gamma_{\rm ph}(t)}{2} & 0 & 0 \\ d_{\rm ph}(t) & V_I(R) - \frac{i\Gamma_{\rm Aug}}{2} + \varepsilon_{\rm ph} - \omega & 0 \\ 0 & V_\gamma & V_F(R) + \varepsilon_{\rm Aug} + \varepsilon_{\rm ph} - \omega \end{pmatrix}. \quad (4)$$

Here $\hat{T}(R)$ is the kinetic energy operator; $V_G(R)$, $V_I(R)$, and $V_F(R)$ are the potential energy curves of the electronic states G, I, and F, respectively (see Fig. 1); $\Gamma_{\rm ph}(t) = 2\pi|d_{\rm ph}(t)|^2$ represents the ground-state photoionization, where $d_{\rm ph}(t) = d_{GI}g_0 g(t, t_0)/2$ is the photoionization matrix element with transition matrix element $d_{GI} = \langle\Phi_G(\mathbf{r}, R)|\hat{x}|\Phi_I^{\varepsilon_{\rm ph}}(\mathbf{r}, R)\rangle$, with the Gaussian envelope $g(t, t_0) = e^{-(t-t_0)^2/\tau^2}$ applied with electric field amplitude g_0, pulse duration τ, and pulse center t_0; and V_γ is the Coulomb matrix element of Auger decay, related to the Auger decay width $\Gamma_{\rm Aug}$ as $\Gamma_{\rm Aug} = \sum 2\pi|V_\gamma|^2$, with γ representing different final dication states. Note that $\Gamma_{\rm ph}$, $\Gamma_{\rm Aug}$, and other related parameters are R dependent in the theory outlined above. For the sake of simplicity, in our numerical simulation we approximate them by their values at molecular equilibrium, which is a rather relevant approximation taking into account high localization of the ground-state vibrational wave function.

The decoupled Hamiltonian (4) and working equation (2) benefit from the local approximation, whose applicability has been verified by many works [48–51]. The local approximation works better for the high-energy electrons [51]. The present model could be extended to the case of several ionic core-excited states, e.g., shake-up or shake-off states [52], with the help of an additional sum over those intermediate states in Eq. (1). Since the photoelectron correlates strongly with a specific ionic core-hole state, these photoelectrons, as well as the corresponding Auger electron, have a rather specific energy and thus could be easily recorded independently in the experiment. As a result, they in fact also can be treated separately for theoretical investigation of the weak-field interaction. Note that in a simple two-level model with only the ground and core-excited states included, when we ignore the Auger decay term, the photoelectron spectrum (PES) $\sigma_{\rm ph}(\varepsilon_{\rm ph})$ on the transition to the ionic state I can be conveniently computed as the norm of the wave packet by integrating over the coordinate R as

$$\sigma_{\rm ph}(\varepsilon_{\rm ph}) = \lim_{t\to\infty}\left\langle\Psi_I^{\varepsilon_{\rm ph}}(R,t)\middle|\Psi_I^{\varepsilon_{\rm ph}}(R,t)\right\rangle. \tag{5}$$

In the final dissociative state V_F, as illustrated in Fig. 1, ion fragments are also released, making such a direct calculation of the PES or AES not possible anymore. Due to this, the technique of the complex absorbing potential (CAP) is applied here by adding a perturbative complex potential $-iW(R) = -i\eta(R - R_c)^3\Theta(R - R_c)$ in the dissociative channel in order to obtain the KER spectra of the ion fragments in coincidence with the AES [53]. Here η is the CAP strength, R_c is the point where the CAP is switched on, and Θ is Heaviside's step function. The KER spectra $\sigma_{\rm KER}(\varepsilon_{\rm ph}, \varepsilon_{\rm Aug}, E)$ can be computed as [42,54,55]

$$\sigma_{\rm KER}(\varepsilon_{\rm ph}, \varepsilon_{\rm Aug}, E) = \frac{1}{\pi}\int_0^\infty\int_0^\infty \left\langle\Psi_F^{\varepsilon_{\rm ph},\varepsilon_{\rm Aug}}(R,t)\middle|W\middle|\right. \times \left.\Psi_F^{\varepsilon_{\rm ph},\varepsilon_{\rm Aug}}(R,t')\right\rangle e^{-iE(t-t')}dt\,dt', \tag{6}$$

where E is the released ion fragment energy. As one can clearly see, the above KER spectra depend on both the photoelectron and Auger electron energies, which implies the necessity of using the proposed photoelectron–Auger electron–ion fragment three-body coincidence spectroscopy, with the energy conservation law $\varepsilon_{\rm ph} + \varepsilon_{\rm Aug} + E = \text{const}$ and accounting for the interaction with ultrashort x-ray free-electron lasers. Note that the above value "const" corresponds to the energy difference between the photon energy and the dissociation limit of a specific dication final state. Equation (6) can also be interpreted as Auger electron–ion fragment two-body joint energy spectra for a monochromatic light with a given photon energy $\varepsilon_{\rm ph}$ and even as one-body KER spectra for a given photon energy $\varepsilon_{\rm ph}$ and Auger energy $\varepsilon_{\rm Aug}$. Moreover, we can also integrate Eq. (6) on the ion fragment energy E in order to obtain the photoelectron–Auger electron joint energy spectra, as

$$\sigma^I_{\text{ph-Aug}}(\varepsilon_{\rm ph}, \varepsilon_{\rm Aug}) = \int \sigma_{\rm KER}(\varepsilon_{\rm ph}, \varepsilon_{\rm Aug}, E)dE. \tag{7}$$

Alternatively, calculations for only one-body Auger electron $\sigma^I_{\rm Aug}(\varepsilon_{\rm Aug})$ or ion fragment KER $\sigma^I_{\rm KER}(E)$ spectra can be implemented by means of corresponding integration as

$$\sigma^I_{\rm KER}(E) = \iint \sigma_{\rm KER}(\varepsilon_{\rm ph}, \varepsilon_{\rm Aug}, E)d\varepsilon_{\rm ph}d\varepsilon_{\rm Aug},$$
$$\sigma^I_{\rm Aug}(\varepsilon_{\rm Aug}) = \iint \sigma_{\rm KER}(\varepsilon_{\rm ph}, \varepsilon_{\rm Aug}, E)d\varepsilon_{\rm ph}dE. \tag{8}$$

Note that since the photoelectron energy depends on both the pump light frequency and energy difference between the states G and I, it would be convenient to define the energy difference $\Delta\varepsilon_I = \omega - \varepsilon_{\rm ph} - (E^I_{v=0} - E^G_{v=0})$ (see Fig. 1), corresponding to the excitation energy with respect to the lowest vibrational state $v = 0$ of state I; here E^X_v $\{X = G, I\}$ is the vibrational energy of state X and $E^I_{v=1} - E^I_{v=0}$ is the energy difference between $v = 0$ and $v = 1$ vibrational states of state I. Apparently, $\Delta\varepsilon_I = 0$ stands for the case when the wave packet is excited from the $v = 0$ of ground state G to the $v = 0$ of the excited state I. Note that $\Delta\varepsilon_I < 0$ can also happen for an ultrashort pump pulse due to its broad bandwidth, when the excitation to $v = 0$ of state I dominates.

III. RESULTS AND DISCUSSION

Our choice of the HF molecule as a showcase was motivated by the presence of a large number of dissociative dication states. Nine final dication states for the HF^{2+} molecule are studied, as shown in Fig. 2. To investigate the dependence of the dynamic effect on the excitation pulse bandwidth, we consider and compare x-ray pulses of $\tau = 1$, 4, and 8 fs. Note that the intensity area of the pulses is constant, ensuring the same small ionization probability (about 1.0%) for all three cases; the peak intensity is about 1.0×10^{13} W/cm^2 for a 1-fs pulse. Due to the present constraint, the contribution from various complex nonlinear effects, such as Rabi oscillations, is negligible. In an experiment, the photoelectron, Auger electron, and ion emitted in the same event can be separated by means of coincidence measurement techniques, providing detailed information on the dynamical features of the system.

It is worth noting that the present theoretical treatment fully takes into account the pump process with a broadband x-ray pulse, as well as the coherent nuclear wave packet of the ionic core-excited state, which is far beyond the conventional sudden approximation (SA) model, where the initial ground wave packet is simply settled and propagated in the

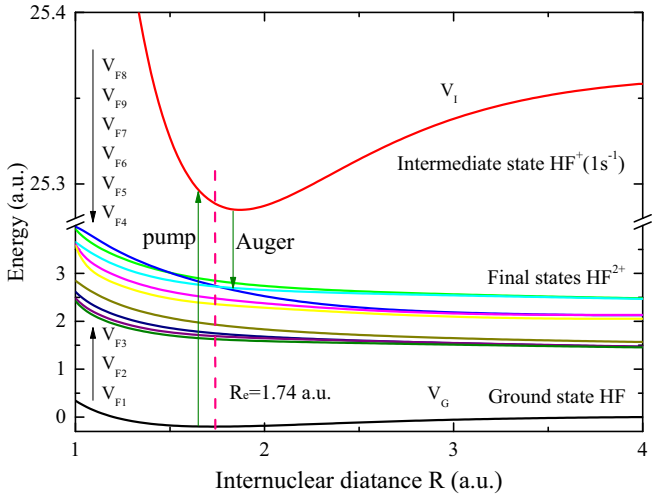

FIG. 2. Potential energy curves of the ground (V_G), core-ionized (V_I), and nine final dicationic states ($V_{F1}, \ldots, V_{F9}$) of the HF molecule, modified from Ref. [56]. The ground-state equilibrium geometry is marked by the pink dashed line. The final dication states are labeled in order of increasing energy at the ground-state equilibrium geometry; the labels $V_{F1}, \ldots, V_{F9}$ correspond to the $1\,^1\Delta$, $1\,^1\Sigma^+$, $1\,^1\Pi$, $2\,^1\Sigma^+$, $1\,^3\Pi$, $1\,^3\Sigma^+$, $2\,^1\Pi$, $3\,^1\Pi$, and $3\,^1\Sigma^+$ states, respectively

core-excited state [57–59]. To simulate the whole dynamic process, we solve Eqs. (2)–(4) using the multiconfigurational time-dependent Hartree method implemented in the Heidelberg package [42,53], but its multiconfigurational aspect is not used since only one nuclear coordinate is involved. For the HF molecule, 161 sin discrete variable representation elements are distributed in the internuclear coordinate range [1.0, 9.0] a.u. of the vibrational degrees of freedom. A CAP is added to the dication dissociation state for the HF molecule through flux analysis with strength $\eta = 0.002$ a.u. and the switch-on point $R_c = 4$ a.u. All potential energy curves are taken from Ref. [56], calculated by the complete active space self-consistent field method with the nonadiabatic coupling included for state $^1\Pi$; the partial Auger decay rates are from Ref. [60], computed by the close-coupling method. The Auger lifetime and vibrational period of the core-excited state are about 3.6 fs ($\Gamma_{\rm Aug} = 0.18$ eV) and 11.8 fs, respectively [56]. The numerical convergence with the chosen parameters has been checked carefully in the calculations.

The photoelectron–Auger electron joint energy spectra of the HF molecule core ionized by the x-ray pulses with varied pulse duration (e.g., bandwidth) are shown in Fig. 3. One can clearly see the dependence of the joint energy map on the bandwidth of the pump pulse. Indeed, the intensity distribution along the photoelectron energy $\Delta\varepsilon_I$ (x axis) of Fig. 3(a) is almost uniform, the fine structure in Fig. 3(b) is becoming more visible, and the fine structure in Fig. 3(c) can be clearly seen. This observation is also confirmed by looking at the (one-body) PES [see the upper panels of Figs. 3(a)–3(c)], which is obtained by integration over the Auger electrons energy. A comparison of the upper panels of Figs. 3(a)–3(c) shows clearly the effect of the spectral broadening due to the increasing pump pulse bandwidth with decreasing pulse duration. When the pulse is relative long [8 fs, Fig. 3(c)], even the vibrational fine structure becomes resolved: One can see clearly three vibrational levels excited in the core-ionized state I with the narrow band pulse, according to the Franck-Condon factor's distribution, which is also presented in Fig. 3(c). When the pulse bandwidth is broad due to a short pulse duration [1 fs, Fig. 3(a)], the vibrational structure is not visible anymore; spectral resolution is lost.

In a similar way, the one-body AES can be obtained with the help of integration of the joint energy maps over the photoelectron energy, as shown in Fig. 3(d). The present Auger electron spectrum includes decay channels from the core-ionized state to the nine final double-ionic states, considered in the present paper. Note that the pink square of the curve in Fig. 3(d) is simulated using the SA model [56] and the

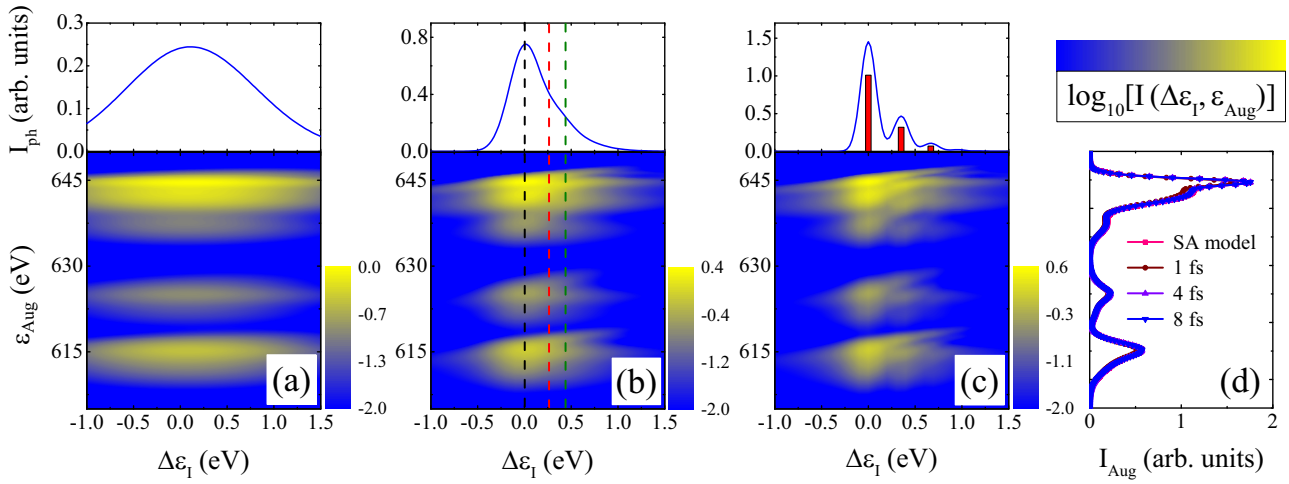

FIG. 3. Photoelectron ($\varepsilon_{\rm ph}$)–Auger electron ($\varepsilon_{\rm Aug}$) joint energy spectra $\sigma^I_{\text{ph-Aug}}(\varepsilon_{\rm ph}, \varepsilon_{\rm Aug})$, triggered by (a) 1-, (b) 4-, and (c) 8-fs pump pulses (lower panels). The upper panels are the PES obtained by integrating $\sigma^I_{\text{ph-Aug}}(\varepsilon_{\rm ph}, \varepsilon_{\rm Aug})$ over Auger electron energy $\varepsilon_{\rm Aug}$; the vertical dashed lines in (b) shows three relative photoelectron energies ($\Delta\varepsilon_I = 0.0$, 0.26, and 0.44 eV) used for the joint energy spectra simulations in Figs. 4 and 5. The relative Franck-Condon factors are also given as a red histogram in (c). (d) The AES, obtained by integrating $\sigma^I_{\text{ph-Aug}}(\varepsilon_{\rm ph}, \varepsilon_{\rm Aug})$ in (a)–(c) over $\Delta\varepsilon_I$ (see the legend). The pink line with a square is the AES computed in the SA model [56].

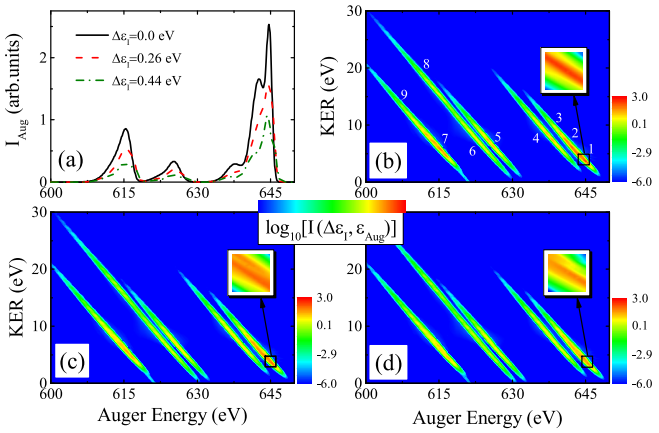

FIG. 4. Auger electron–ion fragment KER joint energy spectra $\sigma_{\mathrm{KER}}(\varepsilon_{\mathrm{ph}}, \varepsilon_{\mathrm{Aug}}, E)$ for (b) $\Delta\varepsilon_I = 0.0\,\mathrm{eV}$, (c) $\Delta\varepsilon_I = 0.26\,\mathrm{eV}$, and (d) $\Delta\varepsilon_I = 0.44\,\mathrm{eV}$ with a pulse duration of 4 fs. The black solid, red dashed, and green dash-dotted lines in (a) correspond to AESs obtained by integration over the KER of the joint energy maps in plots (b), (c), and (d), respectively. The approximate positions of the nine final states in their respective energy regions are marked with numbers (same as in Fig. 2) in (b). The insets in (b)–(d) show a close-up of the coincidence spectral line corresponding to the first state $1\,^1\Delta$.

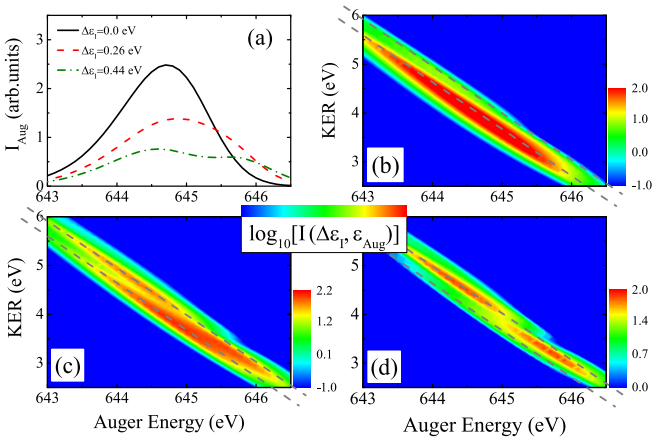

FIG. 5. Same as in Fig. 4 but only the lowest final state $1\,^1\Delta$ is shown. The lower and upper dashed lines in (b)–(d) represent the spectra generated from $\nu = 0$ and 1, respectively, of the core-ionized state $\mathrm{HF}^+(1s^{-1})$.

other three curves correspond to different pump pulse durations (maps in Figs. 3(a)–3(c) integrated in the photoelectron energy range $[-1.0, 1.5]\,\mathrm{eV}$). One can see that the duration (bandwidth) of the pump pulse does not much affect the Auger electron spectra. Moreover, all but the shortest pulse duration case nearly coincide with the AES in the SA model [the pink square of the curve in Fig. 3(d)], corresponding to the interaction with monochromatic light. This can be explained by the fact that in the first-order perturbation theory approximation, which is applicable here, the integration over photoelectron energy eliminates information of the intermediate wave-packet dynamics, as usually summation over unobserved degrees of freedom generally comes with a loss of coherence [61]. In order to retrieve this information from the normal Auger process, complete coincidence information is needed.

Let us now explore the dynamical correlation between the Auger electron energy and the dication fragments' KER, using the pump pulse of an intermediate duration of 4 fs with the three values of the energy detuning $\Delta\varepsilon_I$ from the resonance. Figures 4(b)–4(d) show the two-body AES-KER joint energy maps for the photoelectron relative energy fixed at $\Delta\varepsilon_I = 0.0$, 0.26, and 0.44 eV [see the vertical dashed lines in Fig. 3(b)]. All nine final dicationic states are included in these simulations. Figure 4(a) shows AESs integrated over the KER for the three chosen photoelectron energies (see the legend). For a pulse duration of 4 fs, detuning $\Delta\varepsilon_I = 0.0\,\mathrm{eV}$ corresponds to the main transitions to $\nu = 0$ of the core-ionized state, $\Delta\varepsilon_I = 0.26\,\mathrm{eV}$ has similar transition intensities to both $\nu = 0$ and 1, and $\Delta\varepsilon_I = 0.44\,\mathrm{eV}$ corresponds mainly to the excitation of the $\nu = 1$ vibrational state. Note that we use here the value $\Delta\varepsilon_I = 0.44\,\mathrm{eV}$ instead of the resonant value with the $\nu = 1$ energy level (0.35 eV) in order to suppress contribution from $\nu = 0$. The already integrated AES in Fig. 4(a) shows a strong dependence on the coincidence with a particular energy of the photoelectron, which obviously corresponds to different wave-packet dynamics in the intermediate core-ionized state. Here the three lowest dicationic states ($1\,^1\Delta$, $1\,^1\Sigma^+$, and $1\,^1\Pi$) with KER around 5–10 eV form the strongest AES band in the 640–650 eV energy range. The AES in the interval 630–640 eV is formed mainly by the V_{F4} state $2\,^1\Sigma^+$ with some contribution from the three lowest states. The AES interval 620–630 eV is mainly composed of the two triplet states $1\,^3\Pi$ and $1\,^3\Sigma^+$ (see states V_{F5} and V_{F6} in Fig. 2) with KER around 5 eV. Finally, the lowest-energy band in the AES around 610–620 eV is formed by the three highest dicationic states considered here, $2\,^1\Pi$, $3\,^1\Pi$, and $3\,^1\Sigma^+$, with KER around 5, 20, and 15 eV, respectively.

All the final states show quite similar dissociative properties, which results in a very similar behavior for all of them at the joint energy maps of Figs. 4(b)–4(d). Indeed, those lines follow perfectly the energy conservation law $\varepsilon_{\mathrm{ph}} + \varepsilon_{\mathrm{Aug}} + E = \mathrm{const}$, the energy difference between those lines is the energy difference between different dication potentials in its dissociation limit, or each line corresponds to a dissociation limit. However, a comparison of the joint energy maps [Figs. 4(b)–4(d)] with the integrated AES shows the great advantage of the proposed coincidence spectroscopy: The contribution from different final electronic states can be easily separated from the joint energy maps [see the labels of the final state in Fig. 4(b)]. Moreover, high-resolution measurement would also allow one to see different fine structures of the coincidence lines measured at different $\Delta\varepsilon_I$, which imprints different vibrational wave-packet dynamics in the intermediate core-ionized state [see the insets in Figs. 4(b)–4(d)].

Let us now explore those details by inspecting the joint energy spectra for a single final dicationic state $1\,^1\Delta$ (V_{F1}) shown in Fig. 5. In that case, one is able to see the difference in the fine structure of the joint energy maps obtained at different $\Delta\varepsilon_I$. The lower and upper dashed lines in Figs. 5(b)–5(d) represent the events happening in resonance with $\nu = 0$ and $\nu = 1$ vibrational levels of the intermediate core-ionized state,

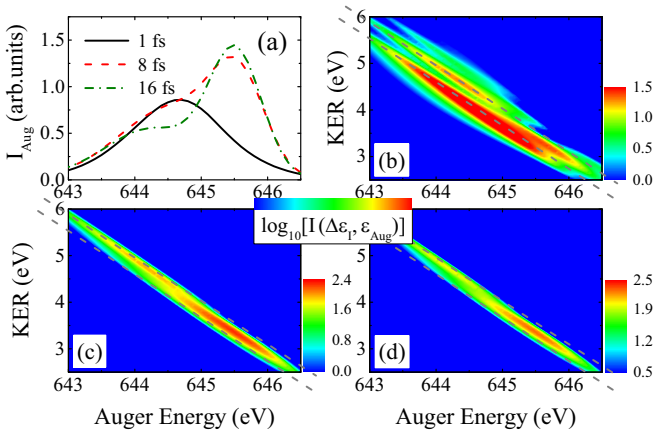

FIG. 6. Auger electron–ion fragment KER joint energy spectra $\sigma_{\mathrm{KER}}(\varepsilon_{\mathrm{ph}}, \varepsilon_{\mathrm{Aug}}, E)$ of only the lowest final state $1^1\Delta$ for $\Delta\varepsilon_I = 0.26\,\mathrm{eV}$ [as in Fig. 5(c)] computed for three different pulse durations of (b) 1 fs, (c) 8 fs, and (d) 16 fs.

respectively. One can see that the joint energy spectra with $\Delta\varepsilon_I = 0$ and 0.44 eV mainly follow the lower and upper dashed lines, respectively, while the one with $\Delta\varepsilon_I = 0.26\,\mathrm{eV}$ shows significant contribution along both upper and lower lines, showing comparable contribution from the $\nu = 0$ and $\nu = 1$ levels.

In the case of $\Delta\varepsilon_I = 0.44\,\mathrm{eV}$ the joint energy spectra following the upper diagonal dashed line show a clear node structure, as a signature of a single-node $\nu = 1$ vibrational wave function of the core-ionized state, appearing according to the reflection principle [62,63]. The one-body AESs shown in Fig. 5(a) also exhibit one-peak and double-peak structures for the cases of $\Delta\varepsilon_I = 0.0$ and 0.44 eV, respectively. It is worth noting that the coincidence spectrum allows one to beat natural lifetime broadening, which affects both AES and PES one-body integrated measurements. Indeed, integrating the joint energy maps along the diagonal line following the energy conservation law ($E + \varepsilon_{\mathrm{Aug}} = \mathrm{const}$, shown by the dashed lines) allows one to observe the vibrational structure with ultrahigh resolution and thus discover the nuclear wave-packet dynamics in the core-ionized state in great detail. A similar effect was previously observed for x-ray-absorption spectra measured in both RAS [64] and resonant inelastic x-ray scattering [63] modes. In the case of Fig. 5(c), when the photoelectron energy corresponds to the excitation between the $\nu = 0$ and $\nu = 1$ vibrational levels of the intermediate state, the clearness of the vibrational structure is masked due to the effect of the lifetime vibrational interference [65]. This case illustrates the creation of a coherent superposition of the core-ionized vibrational states, e.g., the coherent vibrational wave packet.

The Auger electron spectra and AES-KER joint spectra for the fixed $\Delta\varepsilon_I = 0.26\,\mathrm{eV}$ [see Fig. 5(c)] with three different pulse durations 1, 8, and 16 fs for the lowest final state $1^1\Delta$ are shown in Fig. 6. Together with Fig. 5(c) and a duration of 4 fs, the general variations of AESs and AES-KER joint spectra with respect to the pulse duration are clearly presented. With decreasing pulse duration, the widths of AES-KER spectra are broadened, and the vibrational structure in AESs is smeared out by the increasing pulse bandwidth. Furthermore, the joint spectra show that with decreasing pulse duration, the spectral intensity gradually extends from being localized around the two lowest vibrational levels of the core-ionized state (dashed lines) into a much broader energy region. This shows other potential options for manipulation of the core-ionized nuclear wave-packet dynamics with the help of ultrashort x-ray pulses.

The experimental observation of those phenomena as well as extraction of the dynamical information from the joint energy maps would require a high resolution and high statistic measurements for all particles (photoelectron, Auger electron, and fragments from kinetic energy release). These requirements should soon become possible at the modern XFEL facilities due to high photon flux and high repetitions rates, e.g., upon coming in full operation at the European XFEL [66]. With a high-resolution electron time-of-flight spectrometer coupled to an ion velocity mapping spectrometer at the AQS end station SQS beamline at the European XFEL facility, it might be possible to measure electrons with 70 meV resolution at 800 eV kinetic energy and ions with 90 meV resolution at 8 eV kinetic energy, although the efficiency still needs much improvement.

IV. CONCLUSION

In the present paper we suggested a multibody coincidence scheme explored with theoretical simulations performed for the HF molecule core ionized by short x-ray pulses. We considered three-body photoelectron–Auger electron–ion fragment, two-body photoelectron–Auger electron, and Auger electron–KER joint energy maps, as well as single-body photoelectron and Auger electron spectra. Several values of the x-ray pulse duration were used corresponding to different energy bandwidths of the pump pulse. We show that the coincident measurement allows us to get more clearly the fine vibrational structure which cannot be resolved fully in the normal Auger spectrum. It was shown that the Auger electron spectrum is almost independent on the pulse duration. We explored the three-body joint energy maps for the cases when the photoelectron energy was fixed at resonance with the lowest and the first excited vibrational level of the intermediate core-ionized state, as well as in the valley between these states corresponding to their coherent excitation. The results show that the information of the coherent vibrational wave packets can be extracted from the Auger electron energy–KER coincidence spectra. This work provides theoretical guidance and numerical simulation support for the study and manipulation of core-ionized molecular states with ultrashort x-ray pulses. The possibility of the experimental observation was also discussed, in particular at the latest European XFEL facility.

ACKNOWLEDGMENTS

Grants from NSFC (Grants No. 11934004, No. 11974230, and No. 11904192) and National Key Research and Development Program of China (Grant No. 2020YFA0211300) are acknowledged. V.K. acknowledges financial support from the Swedish Research Council (Grant No. 2019-03470).

[1] N. Rohringer and R. Santra, Phys. Rev. A **86**, 043434 (2012).
[2] S. B. Zhang and N. Rohringer, Phys. Rev. A **92**, 043420 (2015).
[3] Q. Bian, Y. Wu, J. G. Wang, and S. B. Zhang, Phys. Rev. A **99**, 033404 (2019).
[4] X. Shi, Y. Wu, J. G. Wang, V. Kimberg, and S. B. Zhang, Phys. Rev. A **101**, 023401 (2020).
[5] N. Rohringer and R. Santra, Phys. Rev. A **77**, 053404 (2008).
[6] J.-C. Liu, Y.-P. Sun, C.-K. Wang, H. Ågren, and F. Gel'mukhanov, Phys. Rev. A **81**, 043412 (2010).
[7] L. S. Cederbaum, Y.-C. Chiang, P. V. Demekhin, and N. Moiseyev, Phys. Rev. Lett. **106**, 123001 (2011).
[8] K. W. D. Ledingham, P. McKenna, and R. P. Singhal, Science **300**, 1107 (2003).
[9] R. Püttner, X.-J. Liu, H. Fukuzawa, T. Tanaka, M. Hoshino, H. Tanaka, J. Harries, Y. Tamenori, V. Carravetta, and K. Ueda, Chem. Phys. Lett. **445**, 6 (2007).
[10] F. Gel'mukhanov, M. Odelius, S. P. Polyutov, A. Föhlisch, and V. Kimberg, Rev. Mod. Phys. **93**, 035001 (2021).
[11] T. Arion and U. Hergenhahn, J. Electron Spectrosc. Relat. Phenom. **200**, 222 (2015).
[12] F. Penent, P. Lablanquie, R. Hall, J. Palaudoux, K. Ito, Y. Hikosaka, T. Aoto, and J. Eland, J. Electron Spectrosc. Relat. Phenom. **144-147**, 7 (2005).
[13] H. W. Haak, G. A. Sawatzky, and T. D. Thomas, Phys. Rev. Lett. **41**, 1825 (1978).
[14] J. Palaudoux, T. Kaneyasu, L. Andric, S. Carniato, G. Gamblin, F. Penent, Y. Hikosaka, E. Shigemasa, K. Ito, S. Fritzsche, E. Kukk, S. Sheinerman, R. F. Fink, P. Lablanquie, and R. Püttner, Phys. Rev. A **98**, 043406 (2018).
[15] T. Arion, R. Püttner, C. Lupulescu, R. Ovsyannikov, M. Förstel, G. Öhrwall, A. Lindblad, K. Ueda, S. Svensson, A. M. Bradshaw, W. Eberhardt, and U. Hergenhahn, J. Electron Spectrosc. Relat. Phenom. **185**, 234 (2012).
[16] J. Viefhaus, G. Snell, R. Hentges, M. Wiedenhöft, F. Heiser, O. Geßner, and U. Becker, Phys. Rev. Lett. **80**, 1618 (1998).
[17] V. Ulrich, S. Barth, S. Joshi, T. Lischke, A. M. Bradshaw, and U. Hergenhahn, Phys. Rev. Lett. **100**, 143003 (2008).
[18] G. Prümper, H. Fukuzawa, D. Rolles, K. Sakai, K. C. Prince, J. R. Harries, Y. Tamenori, N. Berrah, and K. Ueda, Phys. Rev. Lett. **101**, 233202 (2008).
[19] X.-J. Liu, C. Nicolas, M. Patanen, and C. Miron, Sci. Rep. **7**, 2898 (2017).
[20] H. Iwayama and J. R. Harries, J. Electron Spectrosc. Relat. Phenom. **232**, 40 (2019).
[21] S. Song, B. Ding, W. Xu, C. Nicolas, M. Patanen, S. Nandi, J. Bozek, C. Miron, Z. Xiao, and X.-J. Liu, Phys. Rev. A **99**, 022511 (2019).
[22] L. J. Frasinski, K. Codling, and P. A. Hatherly, Science **246**, 1029 (1989).
[23] M. Fushitani, Y. Sasaki, A. Matsuda, H. Fujise, Y. Kawabe, K. Hashigaya, S. Owada, T. Togashi, K. Nakajima, M. Yabashi, Y. Hikosaka, and A. Hishikawa, Phys. Rev. Lett. **124**, 193201 (2020).
[24] P. Emma, R. Akre, J. Arthur, R. Bionta, C. Bostedt, J. Bozek, A. Brachmann, P. Bucksbaum, R. Coffee, F. J. Decker, Y. Ding, D. Dowell, S. Edstrom, A. Fisher, J. Frisch, S. Gilevich, J. Hastings, G. Hays, P. Hering, Z. Huang *et al.*, Nat. Photon. **4**, 641 (2010).
[25] J. Ullrich, A. Rudenko, and R. Moshammer, Annu. Rev. Phys. Chem. **63**, 635 (2012).
[26] M. Harmand, R. Coffee, M. R. Bionta, M. Chollet, D. French, D. Zhu, D. M. Fritz, H. T. Lemke, N. Medvedev, B. Ziaja, S. Toleikis, and M. Cammarata, Nat. Photon. **7**, 215 (2013).
[27] C. Bostedt, S. Boutet, D. M. Fritz, Z. Huang, H. J. Lee, H. T. Lemke, A. Robert, W. F. Schlotter, J. J. Turner, and G. J. Williams, Rev. Mod. Phys. **88**, 015007 (2016).
[28] C. Pellegrini, A. Marinelli, and S. Reiche, Rev. Mod. Phys. **88**, 015006 (2016).
[29] N. Došlić, Phys. Rev. A **74**, 013402 (2006).
[30] D. Baykusheva, P. M. Kraus, S. B. Zhang, N. Rohringer, and H. J. Wörner, Faraday Discuss. **171**, 113 (2014).
[31] P. V. Demekhin, Y.-C. Chiang, and L. S. Cederbaum, Phys. Rev. A **84**, 033417 (2011).
[32] S. B. Zhang and N. Rohringer, Phys. Rev. A **89**, 013407 (2014).
[33] C. Ott, L. Aufleger, T. Ding, M. Rebholz, A. Magunia, M. Hartmann, V. Stooß, D. Wachs, P. Birk, G. D. Borisova, K. Meyer, P. Rupprecht, C. da Costa Castanheira, R. Moshammer, A. R. Attar, T. Gaumnitz, Z.-H. Loh, S. Düsterer, R. Treusch, J. Ullrich *et al.*, Phys. Rev. Lett. **123**, 163201 (2019).
[34] M. J. J. Vrakking, Phys. Rev. Lett. **126**, 113203 (2021).
[35] S. Chatterjee and T. Nakajima, Phys. Rev. A **91**, 043413 (2015).
[36] S. B. Zhang, V. Kimberg, and N. Rohringer, Phys. Rev. A **94**, 063413 (2016).
[37] S. Chatterjee and T. Nakajima, Phys. Rev. A **96**, 063406 (2017).
[38] I. Nam, C.-K. Min, B. Oh, G. Kim, D. Na, Y. J. Suh, H. Yang, M. H. Cho, C. Kim, M.-J. Kim, C. H. Shim, J. H. Ko, H. Heo, J. Park, J. Kim, S. Park, G. Park, S. Kim, S. H. Chun, H. Hyun *et al.*, Nat. Photon. **15**, 435 (2021).
[39] V. Kimberg and N. Rohringer, Struct. Dyn. **3**, 034101 (2016).
[40] V. Zhaunerchyk, M. Mucke, P. Salén, P. van der Meulen, M. Kaminska, R. J. Squibb, L. J. Frasinski, M. Siano, J. H. D. Eland, P. Linusson, R. D. Thomas, M. Larsson, L. Foucar, J. Ullrich, K. Motomura, S. Mondal, K. Ueda, T. Osipov, L. Fang, B. F. Murphy *et al.*, J. Phys. B **46**, 164034 (2013).
[41] E. Pahl, J. Brand, L. S. Cederbaum, and F. Tarantelli, Phys. Rev. A **60**, 1079 (1999).
[42] M. Beck, A. Jackle, G. Worth, and H.-D. Meyer, Phys. Rep. **324**, 1 (2000).
[43] M. U. Kuchiev and S. A. Sheĭnerman, Sov. Phys. Usp. **32**, 569 (1989).
[44] A. Kivimäki, M. Coreno, P. Miotti, F. Frassetto, L. Poletto, C. Stråhlman, M. de Simone, and R. Richter, J. Electron Spectrosc. Relat. Phenom. **209**, 26 (2016).
[45] G. S. Agarwal, Phys. Rev. A **4**, 1778 (1971).
[46] K. Zaheer and M. S. Zubairy, Phys. Rev. A **37**, 1628 (1988).
[47] A. Brown, W. J. Meath, and P. Tran, Phys. Rev. A **63**, 013403 (2000).
[48] L. S. Cederbaum and W. Domcke, J. Phys. B **14**, 4665 (1981).
[49] W. Domcke, Phys. Rep. **208**, 97 (1991).
[50] E. Pahl, H. D. Meyer, and L. S. Cederbaum, Z. Phys. D **38**, 215 (1996).
[51] P. V. Demekhin and L. S. Cederbaum, Phys. Rev. A **83**, 023422 (2011).
[52] E. Shigemasa, T. Gejo, M. Nagasono, T. Hatsui, and N. Kosugi, Phys. Rev. A **66**, 022508 (2002).
[53] G. A. Worth, M. H. Beck, A. Jäckle, O. Vendrell, and H.-D. Meyer, The MCTDH package, Version 8.2 (2000); H.-D. Meyer, The MCTDH package, Version 8.3 (2002); The

MCTDH package, Version 8.4 (2007); O. Vendrell and H.-D. Meyer, The MCTDH package, Version 8.5 (2013); Version 8.5 contains the ML-MCTDH algorithm; current versions are 8.4.18 and 8.5.11 (2019); for the used version see http://mctdh.uni-hd.de/.

[54] Y. R. Liu, Y. Wu, J. G. Wang, O. Vendrell, V. Kimberg, and S. B. Zhang, Phys. Rev. A **102**, 033114 (2020).

[55] Y. R. Liu, V. Kimberg, Y. Wu, J. G. Wang, O. Vendrell, and S. B. Zhang, J. Phys. Chem. Lett. **12**, 5534 (2021).

[56] E. Pahl, H. Meyer, L. S. Cederbaum, D. Minelli, and F. Tarantelli, J. Chem. Phys. **105**, 9175 (1996).

[57] L. Hedin and J. Lee, J. Electron Spectrosc. Relat. Phenom. **124**, 289 (2002).

[58] F. W. Byron and H. M. Foley, Phys. Rev. **134**, A625 (1964).

[59] D. W. Schlitt and C. Stutz, Am. J. Phys. **38**, 70 (1970).

[60] K. Zähringer, H.-D. Meyer, and L. S. Cederbaum, Phys. Rev. A **45**, 318 (1992).

[61] C. Buth and K. J. Schafer, Phys. Rev. A **91**, 023419 (2015).

[62] V. Kimberg, A. Lindblad, J. Söderström, O. Travnikova, C. Nicolas, Y.-P. Sun, F. Gel'mukhanov, N. Kosugi, and C. Miron, Phys. Rev. X **3**, 011017 (2013).

[63] N. Ignatova, V. V. da Cruz, R. C. Couto, E. Ertan, M. Odelius, H. Ågren, F. F. Guimarães, A. Zimin, S. P. Polyutov, F. Gel'mukhanov, and V. Kimberg, Phys. Rev. A **95**, 042502 (2017).

[64] Y. Velkov, Y. Hikosaka, E. Shigemasa, S. Gavrilyuk, and F. Gel'mukhanov, Chem. Phys. Lett. **465**, 153 (2008).

[65] Y. Hikosaka, Y. Velkov, E. Shigemasa, T. Kaneyasu, Y. Tamenori, J. Liu, and F. Gel'mukhanov, Phys. Rev. Lett. **101**, 073001 (2008).

[66] EuXFEL, European XFEL Annual Report 2020 No. XFEL.EU AR-2020, 2021 (unpublished).